

Radio–continuum study of Large Magellanic Cloud Supernova Remnant J0509–6731

L. M. Bozzetto,¹ M. D. Filipović,¹ D. Urošević,^{2,3} R. Kothes,⁴ & E. J. Crawford¹

¹*School of Computing and Mathematics, University of Western Sydney Locked Bag 1797, Penrith South DC, NSW 1797, Australia*

²*Department of Astronomy, Faculty of Mathematics, University of Belgrade, Studentski trg 16, 11000 Belgrade, Serbia*

³*Isaac Newton Institute of Chile, Yugoslavia Branch*

⁴*National Research Council Canada, Herzberg Institute of Astrophysics, Dominion Radio Astrophysical Observatory, P.O. Box 248, Penticton, British Columbia V2A 6J9, Canada*

Released 2011 Xxxxx XX

ABSTRACT

We present a detailed study of Australia Telescope Compact Array (ATCA) observations ($\lambda = 20, 13, 6$ & 3 cm) of supernova remnant (SNR) J0509–6731 in the Large Magellanic Cloud (LMC). The remnant has a ring morphology with brightened regions towards the south-western limb. We also find a second brightened inner ring which is only seen in the radio-continuum. The SNR is almost circular, with a diameter ranging from 7 to 8 pc, and a steep radio spectral index between 36 and 3 cm of $\alpha = -0.73 \pm 0.02$, which is characteristic of younger SNRs. We also report detection of radially orientated polarisation across the remnant at 6 cm, with a mean fractional polarisation level of $P \cong (26 \pm 13)\%$. We find the magnetic field ($\sim 168 \mu\text{G}$) and $\Sigma - D$ ($\Sigma = 1.1 \times 10^{-19} \text{ W m}^{-2} \text{ Hz}^{-1} \text{ sr}^{-1}$, $D = 7.35$ pc) to be consistent with other young remnants.

Key words: polarization – ISM: supernova remnants – Magellanic Clouds – radio continuum: ISM.

1 INTRODUCTION

Supernova remnants (SNRs) play a vital role in the universe, enriching the interstellar medium (ISM) and significantly influences the ISMs evolution, structure and physical properties. The study of SNRs in our own Galaxy is not ideal due to difficulties in estimating accurate distances (which inhibits accurate analysis such as extent and surface brightness) and the high level of absorption in the direction of the Galactic plane. As an alternative, the Large Magellanic Cloud (LMC) at a proximity of 50 kpc (Macri et al. 2006) is a near ideal galaxy for the study of SNRs due to its high active star forming regions (such as 30 Dor) and location outside of the Galactic plane at an angle of 35° (van der Marel & Cioni 2001). Its distance from earth allows us to assume that objects located within are at approximately the same distance, aiding in various analysis methodologies.

In the radio-continuum, SNRs predominately emit non-thermal continuum emission and generally exhibit a spectrum of $\alpha \sim -0.5$ (defined by $S \propto \nu^\alpha$). Although this can vary as there exists a wide variety of SNRs in different stages of evolution and expanding in different environments (Filipovic et al. 1998).

In this paper, we present new radio-continuum observations of SNR J0509–6731, along with archival radio-continuum, X-ray & optical observations. This source was originally classified by Long et al. (1981) as an SNR in their X-ray survey using the Einstein observatory, recording a position of RA (B1950)= $05^h 09^m 28^s$ and DEC (B1950)= $-67^\circ 34' 55''$. Tuohy et al. (1982) estimate a X-ray size of $\sim 25''$, an optical size of $25''$ and estimated a shock velocity of $> 3600 \text{ km s}^{-1}$. No object was found at this position in the 408 MHz image by Clark, Little & Mills (1976). However, reanalysis of the 408 MHz survey data by Tuohy et al. (1982), found weak emission at this point finding a flux density measurement of 95 ± 15 mJy. Tuohy et al. (1982) also observed this object at 5 GHz and measured a flux density of 30 ± 3 mJy. They note that on a surface brightness to diameter ($\Sigma - D$) diagram, SNR J0509–6731 fell below the mean line by a factor of 13 , which is comparable to young Galactic SNRs. They comment that this low $\Sigma - D$ might be a result of differences in the electron acceleration process in Balmer dominated remnants. The remnant is described as a Balmer dominated SNR expanding into a region with a relatively low density ($n_H \leq 0.02^{-3}$) of neutral hydrogen and argue for a Type Ia supernova (SN). Mathewson et al. (1983) measure an X-ray size of $27''$ and a radio spectrum of $\alpha = -0.46$. Fusco-Femiano & Preite-Martinez (1984) esti-

Table 1. Summary of ATCA observations reduced and used in this study.

Date	Scan time (minutes)	Right Ascension	Declination	Array	Frequencies (MHz)	BWidth (MHz)	Chan	Project
2011-Nov-16	49.7	5h 9m 31.00s	-67°31'16.20''	EW367	5,500, 9,000	2048.0	2049	C634 ^a
2011-Nov-15	15.0	5h 9m 31.00s	-67°31'16.20''	EW367	5,500, 9,000	2048.0	2049	C634 ^a
2010-Nov-29	98.0	5h 9m 30.00s	-67°30'60.00''	6A	5,500, 9,000	2048.0	2049	C2367
2010-Nov-28	50.3	5h 9m 30.00s	-67°30'60.00''	6A	5,500, 9,000	2048.0	2049	C2367
2005-Jun-24	819.7	5h 9m 51.48s	-67°16'22.17''	6B	1,384, 1,472	128.0	33	C1395
2005-Apr-18	819.8	5h 9m 51.48s	-67°16'22.17''	1.5A	1,384, 1,472	128.0	33	C1395
1997-Aug-11	643.7	5h 9m 30.00s	-67°30'60.00''	750B	4,800, 4,928	128.0	33	C479
1994-Sep-23	57.0	5h 9m 31.00s	-67°31'15.00''	1.5D	1,380, 2,378	128.0	33	C354
1994-Sep-22	482.3	5h 9m 31.00s	-67°31'15.00''	1.5D	1,380, 2,378	128.0	33	C354
1994-Sep-17	260.7	5h 9m 31.00s	-67°31'15.00''	1.5B	1,380, 2,378	128.0	33	C354

^a – The observing procedure in this project is described in the text.

mates a shock temperature of 3.1 KeV, an age of 900 yr, total swept up mass of 26 M_{\odot} and a shock velocity of 1600 km s⁻¹, which is well below that proposed by Tuohy et al. (1982) of >3600. Mills et al. (1984) record a 843 MHz flux density of 82 mJy, updating the spectral index to -0.48 and also record a surface brightness of >6.4×10²⁰ W m⁻² Hz⁻¹ sr⁻¹. van den Bergh (1988) also argues for a younger remnant, commenting that the small diameter indicates an age of ≤1000 yr. Chu & Kennicutt (1988) give this SNR OB association 400 pc to LH38 and class this remnant as population II. Smith et al. (1991) records a shock velocity >2000 km s⁻¹ and is in agreement with an age of ≤1000 yr. Hughes et al. (1995) notes that there is strong emission of elements from silicon to neon and argues for Type Ia SN. Haberl & Pietsch (1999) record an extent of 9.1'' and give this SNR the association [HP99] 542. Warren & Hughes (2004) confirmed that the SN ejecta had an abundance distribution consistent with Type Ia SN explosion models. They also found that the reverse shock is propagating back into the Fe-rich ejecta and suggests that the brightening in the southwest is due to enhanced density in or a deeper penetration of the reverse shock into the into a portion of the ejecta shell and may be caused enhanced ambient density or intrinsic asymmetry in the explosion itself. Rest et al. (2005) confirmed the Type Ia classification using light echo spectra and also established it as a SN1991T-type energetic event. Additionally, light echo apparent motion was used to estimate the age of the SNR to be 400±120 yr. Arbutina & Urošević (2005) used a 1 GHz flux density of 70 mJy to estimate a surface brightness–diameter of $(\Sigma - D) = (4.2 \times 10^{-20} \text{ W m}^{-2} \text{ Hz}^{-1} \text{ sr}^{-1}, 7 \text{ pc})$. Ghavamian et al. (2007) estimate an age of 295 - 585 yr, a shock velocity of $V_s \geq 4000 \text{ km s}^{-1}$, they detect broad Ly β emission and classify this object as a non-radiative (adiabatic) of Type Ia. Badenes et al. (2008) found an age of ~400 yr, kinetic energy of 1.4×10⁵¹ ergs and concluded that the X-ray properties of SNR J0509–6731 were consistent with models of an energetic 91T-type SN Ia explosion. Seok et al. (2008) states SNR J0509–6731 is thought to be dominated by thermal dust continuum with T(dust) 94±3 K and a Dust mass of 8.7±2.5×10⁻⁵ solar masses. Kosenko et al. (2008) also find that the reverse shock has recently reach the iron layers of the ejecta and are in agreement with previous studies regarding the brightening in the southwest resulting from an asymmetric explosion or density enhancement in the ISM. Models in this study were in good agreement with the observations with circumstellar

density of 3×10⁻²⁵ g/cm³, age of ~400 yr and velocity of ~5000 km s⁻¹. Desai et al. (2010) found no association between this remnant and a YSO, nor the molecular clouds. Schaefer & Pagnotta (2012) found no ex-companion star to a visual magnitude limit of 26.9 within a radius of 1.43'', which they state would infer a double degenerate SN system. Di Stefano & Kilic (2012) and Wheeler (2012) discuss the possibility of this SNR still being the result of a single degenerate explosion.

The observations, data reduction and imaging techniques are described in Section 2. The astrophysical interpretation of newly obtained moderate-resolution total intensity and polarimetric images in combination with archival Chandra X-ray and HST H α observations are discussed in Section 3.

2 OBSERVATIONS AND DATA REDUCTION

Five Australia Telescope Compact Array (ATCA) projects (C1395, C354, C479, C634 and C2367; at wavelengths of 20 cm, 20/13 cm, 6 cm, 6/3 cm and 6/3 cm respectively) were reduced and analysed in this study. A summary of these projects can be seen in Table 1. Project C634 contain our observations of this SNR, which were taken on the 15th and 16th of November 2011. These observations were taken by the ATCA using the CABB receiver with the array configuration EW367, at wavelengths of 3 and 6 cm ($\nu=9000$ and 5500 MHz). The observations were carried out in the so called “snap-shot” mode, totalling ~50 minutes of integration over a 14 hour period. Source PKS B1934-638 was used for primary (flux density) calibration and source PKS B0530-727 was used for secondary (phase) calibration. At 6 cm, the shorter baselines from the EW367 observations were complemented by observations taken from project C2367, which uses a longer baseline array configuration (6A; Table 1), allowing for a higher resolution image. However, we were unable to make use of the 3 cm data from ATCA project C2367 due to strong interference. This lack of data meant we lost the longer baselines and as a result, no high resolution image is available at this wavelength.

The MIRIAD¹ (Sault et al. 1995) and KARMA² (Gooch

¹ <http://www.atnf.csiro.au/computing/software/miriad/>

² <http://www.atnf.csiro.au/computing/software/karma/>

1995) software packages were used for reduction and analysis. More information on the observing procedure and other sources observed in this project can be found in Bozzetto et al. (2012a,b,c, 2013) and de Horta et al. (2012).

Images were formed using MIRIAD multi-frequency synthesis (Sault & Wieringa 1994) and natural weighting. They were deconvolved with primary beam correction applied. The same procedure was used for both U and Q stokes parameter maps.

We measured the flux density of SNR J0509-6731 from 11 separate images between 36 cm and 3 cm, which are summarised in Table 2. We obtain five of these flux density measurements from available mosaics; at 36 cm from the Molonglo Synthesis Telescope (MOST) mosaic image (as described in Mills et al. 1984) and from the SUMMS mosaic image (Mauch et al. 2008), 20 cm from the mosaic by Hughes et al. (2007). We also used 6 cm and 3 cm mosaics published by Dickel et al. (2010). The remaining six measurements were taken from the data reduced and analysed in this study using the projects listed in Table 1. Errors in flux density measurements predominately arose from uncertainties in defining the ‘edge’ of the remnant. However, we estimate these errors to be $<10\%$ (with the exception of the 73 cm measurement, where the associated error is given by Tuohy et al. 1982). Using the flux density measurements in Table 2 (73 – 3 cm), we estimate a spectral index of $\alpha = -0.59$. However, it can be seen that the spectrum breaks at 73 cm, where the recorded flux density is at a level well below that which is expected (by $\sim 50\%$). Low frequency absorption can result in this ‘break’, either through synchrotron self absorption or thermal absorption. A low frequency turnover assumed to be from free-free absorption was found for 7 SNRs in M82 (Wills et al. 1997) at levels comparable to our 408 MHz turnover for SNR J0509-6731. However, M82 has an environment significantly denser than the relatively rarified environment of SNR J0509-6731, and therefore, the turnover is expected to occur at higher frequencies in this denser environment. The more probable explanation for this break is observational effects or an issue with the measurement. Omitting this outlying value from our calculation results in a steeper spectral index with a value of $\alpha = -0.73 \pm 0.02$.

3 RESULTS AND DISCUSSION

SNR J0509-6731 exhibits a ring-like morphology (Fig. 1), centred at RA (J2000)= $05^h 09^m 31.0^s$, DEC (J2000)= $-67^\circ 31' 16.4''$. We estimate the spatial extent of SNR J0509-6731 (Fig. 1) at the 3σ (Table 2; Col. 4) level (0.1 mJy) along the major (NW-SE) and minor (NE-SW) axes (PA= -34°). Its size at 6 cm (5500 MHz) is $31'' \times 29'' \pm 1''$ (8×7 pc with 0.25 pc uncertainty in each direction). We estimate the ring thickness of SNR J0509-6731 to $\sim 6''$ at 6 cm, about 40% of the SNR’s radius.

We find a centrally brightening ring in the interior of this remnant (Fig. 1), something that is not common among SNRs. We estimate the size of this ring at 6 cm to be $16'' \times 12'' \pm 1''$ (4×3 pc with 0.25 pc uncertainty in each direction) at PA= 50° .

There is evident correlation between our 6 cm (5500 MHz) radio-continuum emission and the optical $H\alpha$

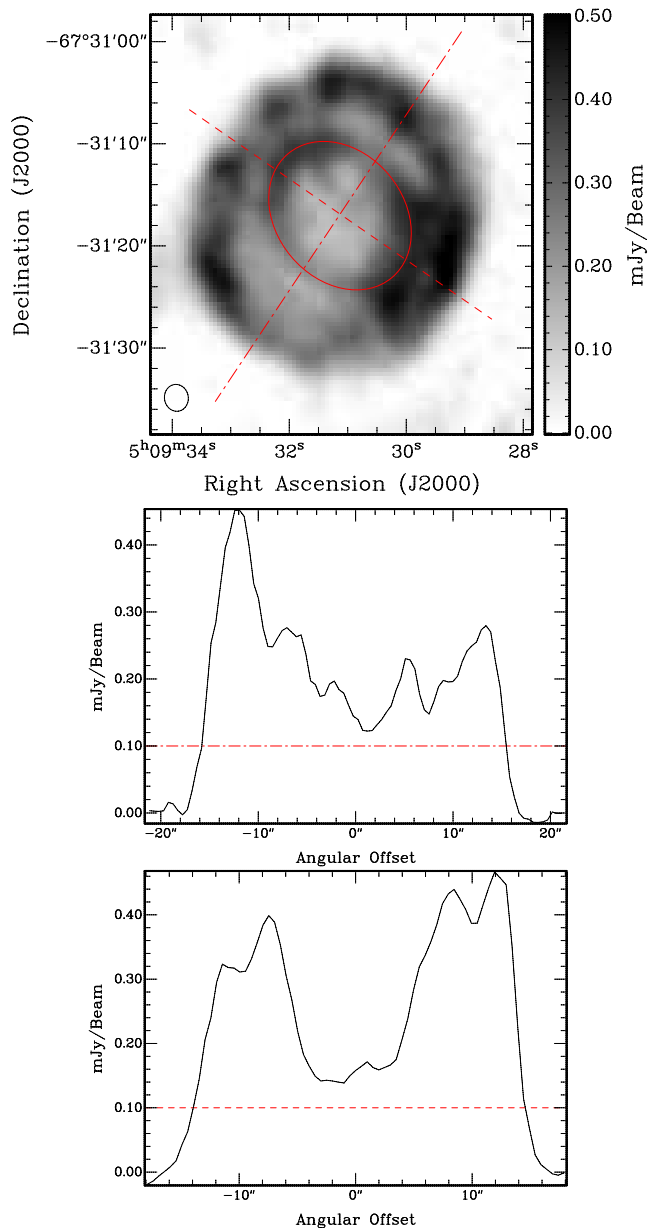


Figure 1. The top image shows the 6 cm intensity image of SNR J0509-6731 overlaid with the approximate major (NW-SE) and minor (NE-SW) axis. The middle and lower images show the 1-dimensional cross-section along the overlaid lines in the top image, with a superimposed line at 3σ .

emission (Hubble Space Telescope; PropID 11015) for this remnant (Fig. 2). This is particularly evident towards the south-western limb of the SNR (where radio emission is the strongest), where we can see the radio 3σ contour closely following the edge of the optical $H\alpha$ emission. The astrometry involved in aligning all images in this paper is within $1''$.

We also find similarities between our 6 cm (5500 MHz) radio-continuum emission and 0.3–7.0 keV X-ray emission (Chandra; observation ID [ObsID] 776³) as seen in Fig. 3.

³ Taken from http://hea-www.harvard.edu/ChandraSNR/snrcat_lmc.html

Table 2. Integrated flux densities of SNR J0509–6731.

λ (cm)	ν (MHz)	ATCA Project	R.M.S (mJy)	Beam Size ($''$)	S_{Total} (mJy)	ΔS_{Total} (mJy)	Reference
73	408	MOST	40	157.3×171.6	95	15	Tuohy et al. (1982)
36	843	MOST ^a	0.4	46.4×43.0	111	11	This work
36	843	SUMMS ^b	1.5	48.5×45.0	109	11	This work
20	1373	C354	0.3	21.2×17.3	73	7	This work
20	1377	C373 ^c	0.7	40.0×40.0	80	8	This work
20	1381	C1395	0.7	13.0×12.2	79	8	This work
13	2377	C354	0.3	12.3×10.1	51	5	This work
6	4800	Multiple ^d	1.0	35.0×35.0	30	3	This work
6	4800	C479	0.3	28.6×11.8	30	3	This work
6	5000	Parkes	—	300×300	30	3	Tuohy et al. (1982)
6	5500	C634, C2367	0.1	2.6×2.3	31	3	This work
3	8640	Multiple ^d	1.0	22.0×22.0	19	2	This work
3	9000	C634	0.2	22.7×16.0	20	2	This work

^a – From the image described in Mills et al. (1984)

^b – From the image described in Mauch et al. (2008)

^c – From the image described in Hughes et al. (2007)

^d – From the image described in Dickel et al. (2010)

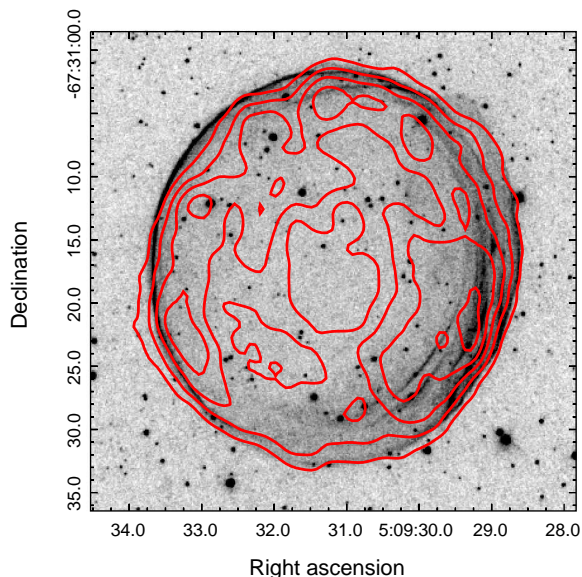


Figure 2. HST $H\alpha$ image of SNR J0509–6731 overlaid with 6 cm ATCA contours. The contours are 3, 6, 9, 12 & 15 σ (where $\sigma = 33 \mu\text{Jy}$).

The optical $H\alpha$ emission shows highly compressed filaments, denoting at high angular resolution the location of the forward shock moving into the ISM, outlying the ellipsoidal shell region interior to which the smooth, low compressed radio and X-ray emission comes.

The non-thermal nature of this remnant in the radio-continuum is confirmed in the spectral energy distribution (SED), shown in Fig. 4, where $\alpha_2 = -0.73 \pm 0.02$. This value is steeper in comparison with typical values of $\alpha = -0.5$ for LMC SNRs (Filipovic et al. 1998) and is more consistent with young SNRs, shown in Table 3. This is in agree-

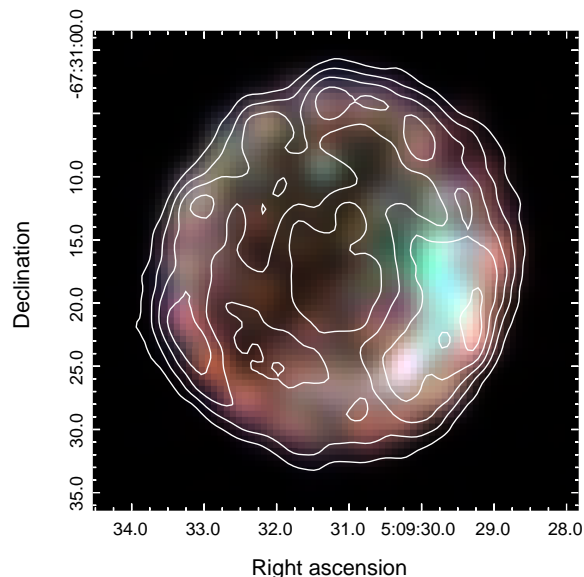


Figure 3. Chandra X-ray colour composite image of SNR J0509–6731 at energy levels 0.3–0.6 keV (red) 0.6–0.95 keV (green) and 0.95–7.0 keV (blue). The image has been smoothed using a gaussian filter ($\sigma = 2$ pixel). ATCA radio contours (at 6 cm) have been overlaid at levels of 3, 6, 9, 12 & 15 σ (where $\sigma = 33 \mu\text{Jy}$).

ment with current estimation of the remnants age, which places it at ~ 400 yr (Rest et al. 2005; Ghavamian et al. 2007; Kosenko et al. 2008; Badenes et al. 2008).

A spectral index map was created between 13 cm and 6 cm (Fig. 5) to show the spacial spectral variations in the remnant. This was achieved by convolving and re-gridding the 6 cm image with the tasks `regrid` and `convol`, to match the size and resolution of the 13 cm image, which had the poorest resolution and thus allowing no oversampling to oc-

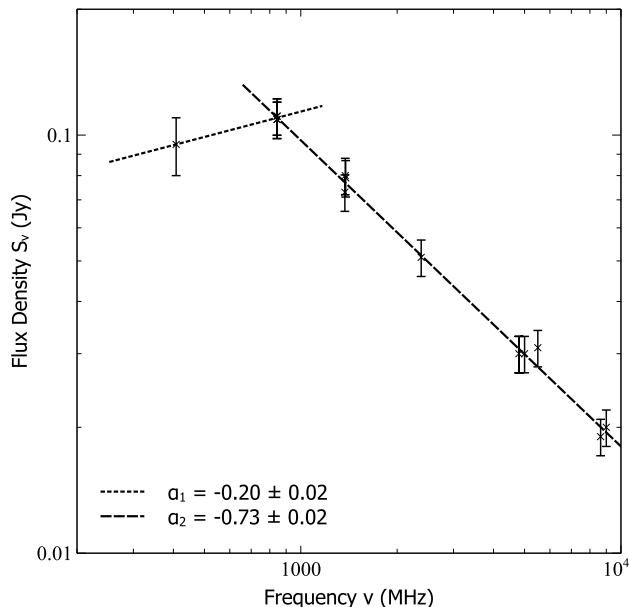


Figure 4. Radio-continuum spectrum of SNR J0509–6731. The markers represent error margins of 10%.

cur. A spectral index map was then created using these maps from both observed frequencies. This was done using the MIRIAD task `maths`, which calculated the spectral index⁴ (α) of each pixel above a level of 3σ . Pixels below this level were blanked in the spectral index map. We note two distinctive and opposite regions of somewhat steeper spectra ($\sim \alpha = -0.7$) marked in yellow around northern and southern regions of the SNR.

A fractional polarisation image was created at 6 cm using Q and U parameters (Fig. 6). A signal-to-noise cut-off of 2σ was used for the Q and U images, while a level of 6σ was used for the intensity image. Values that fall below these cut-off levels are blanked in the output image. The length of the vectors have been reduced by 50% and placed every 1.5 pixels for display purposes. The mean fractional polarisation was calculated using flux density and polarisation:

$$P = \frac{\sqrt{S_Q^2 + S_U^2}}{S_I}$$

where S_Q , S_U and S_I are integrated intensities for the Q , U and I Stokes parameters. We estimate a mean fractional polarisation value of $P = 26 \pm 13\%$ at 6 cm. The magnetic field of the remnant at 6 cm appears to be radially oriented, which is to be expected from Rayleigh-Taylor instabilities in the decelerating remnant (Gull 1975; Chevalier 1976). This is consistent with similarly young SNRs in our own Galaxy, as well as in the LMC (for e.g. those listed in Table 3).

Without reliable polarisation measurements at a second frequency we cannot determine the Faraday rotation and thus cannot deduce the magnetic field strength. However, we make use of the equipartition formula as given by Arbutina et al. (2012) to estimate the magnetic

⁴ spectral index α is defined by $S_\nu = \nu^\alpha$, where S_ν is the integrated flux density and ν is the frequency.

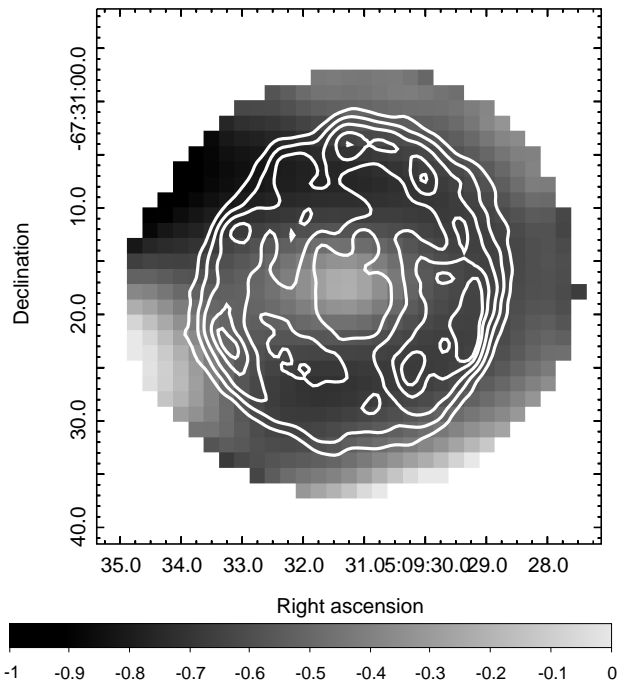


Figure 5. Radio-continuum spectrum map of SNR J0509–6731 between 13 cm and 6 cm. The sidebar quantifies the spectral index scale. ATCA radio contours (at 6 cm) have been overlaid at 3, 6, 9, 12 & 15 σ (where $\sigma = 33 \mu\text{Jy}$).

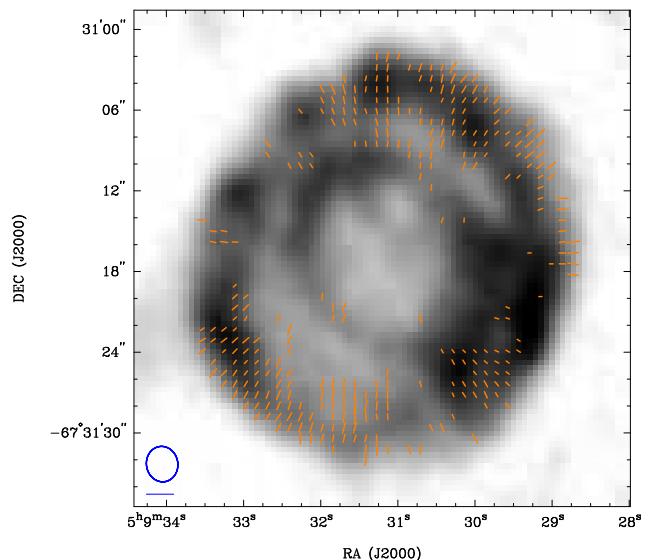


Figure 6. B-field polarisation vectors overlaid on 6 cm ATCA image of SNR J0509–6731. The blue ellipse in the lower left corner represents the synthesised beamwidth of $2.6'' \times 2.3''$ and the blue line below the ellipse represents a polarization vector of 100%.

field strength of this SNR. This formula is based on the Bell (1978) diffuse shock acceleration (DSA) theory. This derivation is purely analytical, accommodated especially for the estimation of magnetic field strength in SNRs. The average equipartition field over the whole shell of SNR J0509–6731 is $\sim 168 \mu\text{G}$ with an estimated minimum

Table 3. Comparison of SNR J0509–6731 to similar remnants.

Name	Age (yr)	α^*	P (%)	P_λ (cm)	Reference
0509–67.5	~ 400	-0.73	26 ± 13	6	This work
Cassiopeia A	—	-0.77	8-10	6	Anderson et al. (1995)
Tycho	~ 441	-0.65	20-30 ^a	6	Dickel et al. (1991)
Kepler	~ 409	-0.64	6	6	DeLaney et al. (2002)
SN 1006	~ 1000	-0.6	17 ^d	20	Reynoso et al. (2013)
N132D	$\sim 2500^b$	-0.70	4	6	Dickel & Milne (1995)
0519–6902	$\sim 600^c$	-0.53	2	6	Bozzetto et al. (2012c)

* – Galactic spectral indices came from the catalogue by Green (2009).

^a – Based on the mean polarisation found for the brightened limbs

^b – Vogt & Dopita (2011)

^c – Borkowski et al. (2006)

^d – Higher polarisation (near the theoretical limit of $\sim 70\%$) was found in regions of weaker radio emission.

energy of $E_{min} = 1.2 \times 10^{49}$ ergs (see Arbutina et al. (2012); and corresponding “calculator”⁵). This value is typical of young SNRs with a strongly amplified magnetic field.

The position of SNR J0509–6731 at the surface brightness to diameter ($\Sigma - D$) diagram ($\Sigma = 1.1 \times 10^{-19}$ W m⁻² Hz⁻¹ sr⁻¹, $D = 7.35$ pc) by Berezhko & Völk (2004), suggests that this remnant is in the transition phase between late free expansion and early Sedov phase, with an explosion energy of $\sim 0.25 \times 10^{51}$, which evolves in an environment with a density of ~ 0.3 cm⁻³. This estimate of minimum explosion energy is lower than that found by Badenes et al. (2008) who found a value of 1.40×10^{51} , a result of using different models. Our estimate of surface brightness is comparable to values found for galactic remnants in rarified environments, such as Tycho’s SNR ($\Sigma = 1.32 \times 10^{-19}$ W m⁻² Hz⁻¹ sr⁻¹, $D = 9.3$ pc) and Kepler’s SNR ($\Sigma = 3.18 \times 10^{-19}$ W m⁻² Hz⁻¹ sr⁻¹, $D = 5.2$ pc) (Pavlović et al. 2013).

4 CONCLUSION

We have used observations taken by the ATCA to carry out a detailed radio continuum study on SNR J0509–6731. With a size of only $D \cong 8 \times 7$ pc, SNR J0509–6731 is one of the smallest remnants currently known in the LMC. We find a relatively steep spectrum of ($\alpha = -0.73 \pm 0.02$) and relatively strong magnetic field of $168 \mu\text{G}$, which is characteristic of a young remnant (e.g. Jiang et al. 2013). Its small size also sets this SNR apart from typical $\Sigma - D$ values of SNRs at $\Sigma = 1.1 \times 10^{-19}$ W m⁻² Hz⁻¹ sr⁻¹, $D = 7.35$ pc, though, still in close proximity to another Balmer dominated LMC SNR, SNR J0519–6902. This SNR shares the same radially orientated polarisation as other young Type Ia remnants, with a mean fractional polarisation level of $P = (26 \pm 13)\%$.

ACKNOWLEDGEMENTS

The Australia Telescope Compact Array is part of the Australia Telescope which is funded by the Commonwealth of Australia for operation as a National Facility managed by

CSIRO. This research is supported by the Ministry of Education and Science of the Republic of Serbia through project No. 176005.

REFERENCES

- Anderson M. C., Keohane J. W., Rudnick L., 1995, ApJ, 441, 300
- Arbutina B., Urošević D., 2005, MNRAS, 360, 76
- Arbutina B., Urošević D., Andjelić M. M., Pavlović M. Z., Vukotić B., 2012, ApJ, 746, 79
- Badenes C., Hughes J. P., Cassam-Chenaï G., Bravo E., 2008, ApJ, 680, 1149
- Bell A. R., 1978, MNRAS, 182, 443
- Berezhko E. G., Völk H. J., 2004, A&A, 427, 525
- Borkowski K. J., Williams B. J., Reynolds S. P., Blair W. P., Ghavamian P., Sankrit R., Hendrick S. P., Long K. S., Raymond J. C., Smith R. C., Points S., Winkler P. F., 2006, ApJ, 642, L141
- Bozzetto L. M., Filipović M. D., Crawford E. J., Haberl F., Sasaki M., Urošević D., Pietsch W., Payne J. L., de Horta A. Y., Stupar M., Tothill N. F. H., Dickel J., Chu Y.-H., Gruendl R., 2012a, MNRAS, 420, 2588
- Bozzetto L. M., Filipovic M. D., Crawford E. J., Payne J. L., de Horta A. Y., Stupar M., 2012b, Rev. Mexicana Astron. Astrofis., 48, 41
- Bozzetto L. M., Filipović M. D., Crawford E. J., Sasaki M., Maggi P., Haberl F., Urošević D., Payne J. L., De Horta A. Y., Stupar M., Gruendl R., Dickel J., 2013, MNRAS, 432, 2177
- Bozzetto L. M., Filipovic M. D., Urošević D., Crawford E. J., 2012c, Serbian Astronomical Journal, 185, 25
- Chu Y.-H., Kennicutt Jr. R. C., 1988, AJ, 96, 1874
- de Horta A. Y., Filipović M. D., Bozzetto L. M., Maggi P., Haberl F., Crawford E. J., Sasaki M., Urošević D., Pietsch W., Gruendl R., Dickel J., Tothill N. F. H., Chu Y.-H., Payne J. L., Collier J. D., 2012, A&A, 540, A25
- DeLaney T., Koralesky B., Rudnick L., Dickel J. R., 2002, ApJ, 580, 914
- Desai K. M., Chu Y.-H., Gruendl R. A., Dluger W., Katz M., Wong T., Chen C.-H. R., Looney L. W., Hughes A., Muller E., Ott J., Pineda J. L., 2010, AJ, 140, 584
- Di Stefano R., Kilic M., 2012, ApJ, 759, 56

⁵ The calculator is available at <http://poincare.matf.bg.ac.rs/~arbo/eqp/>

- Dickel J. R., McIntyre V. J., Gruendl R. A., Milne D. K., 2010, *AJ*, 140, 1567
- Dickel J. R., Milne D. K., 1995, *AJ*, 109, 200
- Dickel J. R., van Breugel W. J. M., Strom R. G., 1991, *AJ*, 101, 2151
- Filipovic M. D., Pietsch W., Haynes R. F., White G. L., Jones P. A., Wielebinski R., Klein U., Dennerl K., Kahabka P., Lazendic J. S., 1998, *A&AS*, 127, 119
- Fusco-Femiano R., Preite-Martinez A., 1984, *ApJ*, 281, 593
- Ghavamian P., Blair W. P., Sankrit R., Raymond J. C., Hughes J. P., 2007, *ApJ*, 664, 304
- Gooch R., 1995, in Shaw R. A., Payne H. E., Hayes J. J. E., eds, *Astronomical Data Analysis Software and Systems IV Vol. 77 of Astronomical Society of the Pacific Conference Series*, Space and the Spaceball. p. 144
- Green D. A., 2009, *Bulletin of the Astronomical Society of India*, 37, 45
- Haberl F., Pietsch W., 1999, *A&AS*, 139, 277
- Hughes A., Staveley-Smith L., Kim S., Wolleben M., Filipović M., 2007, *MNRAS*, 382, 543
- Hughes J. P., Hayashi I., Helfand D., Hwang U., Itoh M., Kirshner R., Koyama K., Markert T., Tsunemi H., Woo J., 1995, *ApJ*, 444, L81
- Jiang Z. J., Zhang L., Fang J., 2013, *MNRAS*, 433, 1271
- Kosenko D., Vink J., Blinnikov S., Rasmussen A., 2008, *A&A*, 490, 223
- Long K. S., Helfand D. J., Grabelsky D. A., 1981, *ApJ*, 248, 925
- Macri L. M., Stanek K. Z., Bersier D., Greenhill L. J., Reid M. J., 2006, *ApJ*, 652, 1133
- Mathewson D. S., Ford V. L., Dopita M. A., Tuohy I. R., Long K. S., Helfand D. J., 1983, *ApJS*, 51, 345
- Mauch T., Murphy T., Buttery H. J., Curran J., Hunstead R. W., Piestrzynski B., Ropbertson J. G., Sadler E. M., 2008, *VizieR Online Data Catalog*, 8081, 0
- Mills B. Y., Turtle A. J., Little A. G., Durdin J. M., 1984, *Australian Journal of Physics*, 37, 321
- Pavlović M. Z., Urošević D., Vukotić B., Arbutina B., Göker Ü. D., 2013, *ApJS*, 204, 4
- Rest A., Suntzeff N. B., Olsen K., Prieto J. L., Smith R. C., Welch D. L., Becker A., Bergmann M., Clocchiatti A., Cook K., Garg A., Huber M., Miknaitis G., Minniti D., Nikolaev S., Stubbs C., 2005, *Nature*, 438, 1132
- Reynoso E. M., Hughes J. P., Moffett D. A., 2013, *AJ*, 145, 104
- Sault R. J., Teuben P. J., Wright M. C. H., 1995, in Shaw R. A., Payne H. E., Hayes J. J. E., eds, *Astronomical Data Analysis Software and Systems IV Vol. 77 of Astronomical Society of the Pacific Conference Series*, A Retrospective View of MIRIAD. p. 433
- Sault R. J., Wieringa M. H., 1994, *A&AS*, 108, 585
- Schaefer B. E., Pagnotta A., 2012, *Nature*, 481, 164
- Seok J. Y., Koo B.-C., Onaka T., Ita Y., Lee H.-G., Lee J.-J., Moon D.-S., Sakon I., Kaneda H., Lee H. M., Lee M. G., Kim S. E., 2008, *PASJ*, 60, 453
- Smith R. C., Kirshner R. P., Blair W. P., Winkler P. F., 1991, *ApJ*, 375, 652
- Tuohy I. R., Dopita M. A., Mathewson D. S., Long K. S., Helfand D. J., 1982, *ApJ*, 261, 473
- van den Bergh S., 1988, *ApJ*, 327, 156
- van der Marel R. P., Cioni M.-R. L., 2001, *AJ*, 122, 1807
- Vogt F., Dopita M. A., 2011, *Ap&SS*, 331, 521
- Warren J. S., Hughes J. P., 2004, *ApJ*, 608, 261
- Wheeler J. C., 2012, *ApJ*, 758, 123
- Wills K. A., Pedlar A., Muxlow T. W. B., Wilkinson P. N., 1997, *MNRAS*, 291, 517